Boundary-layer analysis for natural convection in a vertical porous layer filled with a non-Newtonian fluid

W. Bian, P. Vasseur and E. Bilgen
Mechanical Engineering Department, Ecole Polytechnique, Montreal, Canada

An analytical and numerical study is reported of steady-state natural convection in a two-dimensional rectangular porous cavity saturated by a non-Newtonian fluid. The enclosure is heated and cooled isothermally from the vertical sides, while the horizontal walls are adiabatic. The modified Darcy power-law model proposed by Pascal (1983) is used to characterize the non-Newtonian fluid behavior. In the large Rayleigh number limit, the boundary-layer equations are solved analytically upon introducing a similarity transformation. The core structure is determined using an integral form of the energy equation. Numerical integrations are carried out using the Runge–Kutta method. Solutions for the flow and temperature fields and Nusselt numbers are obtained in terms of a modified Rayleigh number R, the aspect ratio of the cavity A, and the power-law index n. A numerical study of the same phenomenon, obtained by solving the complete system of governing equations, is also conducted, and results are reported in the range $10^2 \leq R \leq 10^3$, $4 \leq A \leq 8$, and $0.6 \leq n \leq 1.4$. The numerical experiments confirm the flow features and scales anticipated by the approximate boundary-layer solution.

Keywords: natural convection; porous media; non–Newtonian fluid

Introduction

Buoyancy-induced convection in a fluid-saturated porous medium is of considerable interest, owing to several geophysical and engineering applications. Over the last two decades, much work has been done on this topic. A problem of fundamental interest that has received attention from many investigators is that of natural convection in confined enclosures driven by horizontal temperature gradients. Analytical works reported include boundary-layer analyses by Weber (1975), Walker and Homsy (1978), and Bejan (1979). Simpkins and Blythe (1980) have presented integral solutions, whereas approximate solutions have been obtained by Walker and Homsy (1978) and Bejan and Tien (1978). Much of this activity, both numerical and experimental, has been summarized in a recent book by Nield and Bejan (1992).

Studies on flow in non-Newtonian fluid-saturated porous media, on the other hand, have only just begun, stimulated by a broad range of applications such as chemical reactor design, polymer engineering, certain separation processes, geophysical systems, ceramic processing, enhanced oil recovery, and filtration. One of the first studies of natural convection of non-Newtonian fluids in porous media was conducted by Chen and Chen (1987) who considered a power-law fluid adjacent to an impermeable horizontal plate heated with a nonuniform heat flux. In subsequent papers, these authors extended their work to include the cases of a horizontal plate with a prescribed temperature variation (1988a) and an isothermal vertical plate (1988b). They used the power-law model suggested by Christopher and Middleman (1965) and later modified by Dharmadhikari and Kale (1985). On the basis of the boundary-layer approximation, the effect of the power-law index n on the heat transfer characteristics was discussed. The rheological effects of power-law fluid with a yield stress on the natural convection mechanism over a heated vertical cylinder embedded in a porous medium were considered by Pascal and Pascal (1989). The cases of constant temperature boundary and constant heat-flux boundary, along the heated vertical cylinder, were analyzed. From approximate similarity solutions obtained in a closed form, these authors demonstrated that the resulting temperature and velocity profiles are not the same as in the Newtonian-fluid case. They also demonstrated that the onset of natural convection occurs, provided that certain inequalities, which depend strongly on the yield stress, are satisfied. The buoyancy-induced flows of non-Newtonian fluids over nonisothermal bodies of arbitrary shape within saturated porous media were considered by Nakayama and Koyama (1991). Using the power-law model of Dharmadhikari and Kale (1985) and introducing a general similarity transformation, the governing equations for the flow and transport around a nonisothermal body of arbitrary shape were reduced to a set of ordinary differential equations. It can be shown that any plane or axisymmetrical body of arbitrary shape possesses a corresponding family of surface wall temperature distributions that permit similarity solutions. Recently, non-Newtonian Couette flow through inelastic fluid-saturated porous media due to a moving plate boundary have been investigated analytically by Nakayama (1992). The momentum equation, which includes both the viscous (Brinkman) and inertia (Forchheimer) terms, was solved to examine the effects of the pseudoplasticity, boundary friction, and porous inertia on the velocity profile and the shear stress at the moving wall. It was found that the effects of the Darcy number (boundary frictional

Address reprint requests to Professor Bian at the Mechanical Engineering Department, Ecole Polytechnique, C.P. 6079, Succ. 'Centre-Ville,' Montreal, Canada H3C 3A7.

Received 1 February 1994; accepted 2 May 1994

effect) and the power-law index n are very much alike in the sense that the decrease of these parameters results in thinning of the velocity boundary layer. The effect of the Forchheimer term (inertial effect) is to reduce the velocity throughout the porous medium.

All the above studies are concerned with the problem of natural convection of a non-Newtonian fluid through an unbounded porous medium. On the other hand, heat transfer by natural convection across enclosures has been studied less. The only available investigation on this flow configuration is provided by Amari et al. (1993). The case of a rectangular enclosure heated from the bottom or by the side was considered by these authors, using the power-law model proposed by Pascal (1983). An approximate analytical solution, valid for shallow cavities, was derived on the basis of a parallel flow configuration and an integral form of the energy equation. Solutions for the flow and temperature fields and for the Nusselt number were obtained explicitly in terms of a modified Rayleigh number and the power-law index. A numerical study of the same phenomenon, obtained by solving the complete system of governing equations, was also conducted. Good agreement was found between the analytical prediction and the numerical simulation. Recently, Bian et al. (1993) have extended this study to the case of an inclined cavity.

The main objective of this paper is to address the question of implications of the rheological effects on the natural convection heat transfer within a vertical rectangular porous enclosure heated isothermally from the side. The power-law model proposed by Pascal (1983) is used to characterize the non-Newtonian fluid behavior. Using the boundary-layer approximations, the resulting simplified governing equations are solved using a similarity transformation and an integral form of the energy equation. The structure of the flow and the heat transfer through the cavity is obtained in terms of a modified Rayleigh number, power-law index, and aspect ratio of the enclosure. A numerical study of the same phenomenon, obtained by solving the complete system of governing equations, is also conducted. The results presented here are relevant to a better understanding of the general flow and heat transfer characteristics of non-Newtonian flows in porous media.

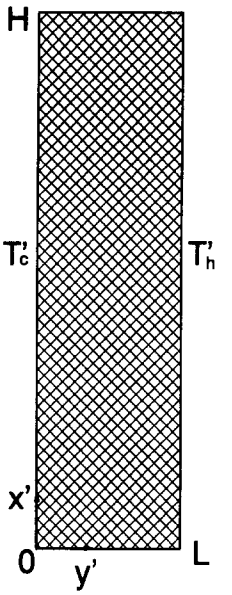

Figure 1 Definition sketch of the problem

Governing equations

The problem under consideration is shown in Figure 1. A two-dimensional (2-D) vertical rectangular enclosure is filled with a homogeneous isotropic porous medium saturated by a non-Newtonian power-law fluid. Both horizontal boundaries are adiabatic, and the vertical boundaries are held at constant

Notation

A	Aspect ratio of the cavity, H/L
a	Coefficient, Equation 22
B^*	Coefficient, Equation 33
b	Coefficient, Equation 22
c	Integration constant, Equation 26
d	Coefficient, Equation 29
g	Acceleration due to gravity
H	Height of the cavity
k	Thermal conductivity of fluid-saturated porous medium
K	Permeability of the porous medium
L	Length of the cavity
l	Characteristic length in the boundary-layer regime
n	Power-law index
Nu	Nusselt number, Equation 7
p'	Pressure
q'	Heat transfer rate
R	Modified Rayleigh number, $K\rho g\beta\Delta T'(L/\alpha)^n/\varepsilon$
T'	Temperature
$\Delta T'$	Temperature difference $T'_h - T'_c$
$\vec{V}'$	Superficial velocity
u'	Superficial velocity in the x'-direction
v'	Superficial velocity in the y'-direction
x', y'	Coordinates

Greek symbols

α	Effective thermal diffusivity
β	Coefficient of thermal expansion
δ^*	Dimensionless thickness of the boundary layer
ε	Parameter in power-law model, Equation 3
η	Similarity variable
θ	Dimensionless temperature
μ	Dynamic viscosity for a Newtonian fluid
μ'_a	Apparent viscosity for a power-law fluid, Equation 3
ρ	Density
ϕ	Porosity of porous media
ψ	Dimensionless stream function

Superscripts

$'$	Dimensional quantities
$*$	Dimensionless quantities

Subscripts

c	Cold wall
h	Hot wall
o	Core region
max	Maximum value

temperatures T_c' and T_h'. The cavity is of height H and width L. It is assumed that the fluid and the porous medium are everywhere in local thermodynamic equilibrium and the properties of the fluid and porous medium are constant. The governing equations for the conservation of momentum and energy in the Darcy regime and with the Boussinesq approximation are given by (Amari et al. 1993)

$$\nabla^2\psi^* = -\frac{1}{\mu_a^*}\left(\frac{\partial\psi^*}{\partial x^*}\frac{\partial\mu_a^*}{\partial x^*} + \frac{\partial\psi^*}{\partial y^*}\frac{\partial\mu_a^*}{\partial y^*} - R\frac{\partial T^*}{\partial y^*}\right) \tag{1}$$

$$\nabla^2 T^* = u^*\frac{\partial T^*}{\partial x^*} + v^*\frac{\partial T^*}{\partial y^*} \tag{2}$$

$$\mu_a^* = \frac{\mu_a'}{\varepsilon(\alpha/L)^{n-1}} = (u^{*2} + v^{*2})^{n-1/2} \tag{3}$$

where μ_a^* is the dimensionless apparent viscosity, n the power-law index, ε a parameter in the power-law model given by (Pascal 1983)

$$\varepsilon = \frac{2\mu}{8^{n+1/2}(K\phi)^{n-1/2}(n/(1+3n))^n}$$

and $R = K\rho g\beta(T_h' - T_c')(L/\alpha)^n/\varepsilon$ is a modified Rayleigh number for flow of non-Newtonian fluids through a porous medium. All other symbols are defined in the nomenclature, and primes denote dimensional quantities.

In Equation 1, ψ^* is a dimensionless stream function and is defined as

$$u^* = \frac{\partial\psi^*}{\partial y^*} \qquad v^* = -\frac{\partial\psi^*}{\partial x^*} \tag{4}$$

such that the equation of continuity is identically satisfied.

The governing equations have been reduced to dimensionless forms by using the following scales: L for length, α/L for velocity, and $\Delta T = T_h' - T_c'$ for temperature.

The nondimensional boundary conditions over the walls of the enclosure are

$$\psi^* = 0, \quad T^* = 0, \quad \text{on } y^* = 0 \tag{5a}$$

$$\psi^* = 0, \quad T^* = 1, \quad \text{on } y^* = 1 \tag{5b}$$

$$\psi^* = 0, \quad \frac{\partial T^*}{\partial x^*} = 0, \quad \text{on } x^* = 0, A \tag{5c}$$

where $A = H/L$ is the cavity aspect ratio.

Equations 1 to 4, together with the boundary conditions (Equation 5), complete the problem definition. The solution is dependent on the parameters R, A, and n. In the following sections, we report a boundary-layer solution of the kind developed by Simpkins and Blythe (1980), and a numerical solution, which is able to handle the complete form of the governing equations.

Boundary-layer solution

When the modified Darcy–Rayleigh number is large, the flow is characterized by thin thermal boundary layers adjacent to the vertical walls. The vertical boundary layers are governed by Equations 1 to 4. The scales recommended by these equations can be found based on the method of scale analysis. This analysis will be presented first, and then an approximate solution for the boundary-layer momentum and energy equations will be discussed.

At sufficiently high Rayleigh numbers, the flow will have a boundary-layer core structure consisting of a core region and two vertical boundary layers. In this regime, along the two vertical walls, $u^* \gg v^*$, and the apparent viscosity μ_a^* has the approximate relation $\mu_a^* \sim u^{*(n-1)}$. Following the scale analysis presented by Weber (1975) for the natural convection of a Newtonian fluid in a vertical porous layer, it is readily found from Equations 1 and 2 and boundary conditions (Equation 5) that

$$\begin{aligned} &\delta^* \sim A^{1/2}R^{-1/2n} \\ &\psi^* = A^{1/2}R^{1/2n} \\ &u \sim R^{1/n}, \quad v^* \sim A^{-1/2}R^{1/2n} \\ &\mathrm{Nu} \sim A^{-1/2}R^{1/2n} \end{aligned} \tag{6}$$

where δ^* is the dimensionless thickness of the horizontal boundary layer and Nu is the Nusselt number defined as the ratio of total heat transfer over the heat transfer by pure conduction:

$$\mathrm{Nu} = \frac{q'}{q_c'} \tag{7}$$

From the scales of the boundary flow recommended by the scale analysis, it is convenient to renormalize the governing equations by introducing the following transformations:

$$x = x^*A, \quad y = y^*R^{1/2n}, \quad \psi = \psi^*R^{-1/2n}, \quad T = T^* \tag{8}$$

Substituting the above variables into Equations 1 to 3 and making the usual boundary-layer approximations, it is found that the dimensionless boundary-layer equations are

$$\frac{\partial}{\partial y}\left(\frac{\partial\psi}{\partial y}\right)^n = \frac{\partial T}{\partial y} \tag{9}$$

$$\frac{\partial\psi}{\partial y}\frac{\partial T}{\partial x} - \frac{\partial\psi}{\partial x}\frac{\partial T}{\partial y} = \frac{\partial^2 T}{\partial y^2} \tag{10}$$

Since the temperature and fluid fields are centrosymmetrical (Gill 1966), only one boundary layer needs to be considered. Also, the temperature and stream functions in the core region are assumed to be a function of x only. We choose the boundary layer along the cold wall and establish the necessary boundary conditions for the above equations:

$$\psi = 0, \quad T = 0, \quad \text{at } y = 0 \tag{11a}$$

$$\psi = \psi_o(x), \quad T = T_o(x), \quad \text{at } y \to \infty \tag{11b}$$

where $\psi_o(x)$ and $T_o(x)$ are the dimensionless stream function and temperature distributions within the core of the cavity, respectively.

For the special case of a Newtonian fluid ($n = 1$), Weber (1975) solved Equations 9 and 10 by using the modified Oseen method. However, this technique cannot be used here owing to the nonlinearity involved in Equation 9. A consistent boundary-layer method, valid for non-Newtonian fluids, is proposed as follows.

Equations 9 and 10 are first transformed by introducing the following similarity variables:

$$\psi = T_o^{1/n}f(x,\eta), \quad \frac{T - T_o(x)}{T_o(x)} = -\theta(x,\eta) \tag{12}$$

where $\eta = \dfrac{y}{x^{1/2}}T_o^{1/2n}$ is the proposed similarity variable.

The above transformations are similar to those employed by Nakayama and Koyama (1991) in the study of the free-convection flow of non-Newtonian fluids along a nonisothermal body.

Using the above transformed coordinates, Equations 9 and 10 and the boundary conditions (Equation 11) can be expressed

as

$$(f')^n = \theta \tag{13}$$

$$\theta'' + \frac{f\theta'}{2}\left[1 + \frac{I(x)}{n}\right] - f'\theta I(x) = x\left[f'\frac{\partial\theta}{\partial x} - \theta'\frac{\partial f}{\partial x}\right] - f'I(x) \tag{14}$$

where

$$I(x) = \frac{x}{T_o}\frac{dT_o}{dx} = \frac{d\ln T_o}{d\ln x} \tag{15}$$

with the boundary conditions

$$f = 0, \quad \theta = 1, \quad \text{at } \eta = 0 \tag{16a}$$

$$\theta = 0, \quad \text{at } \eta \to \infty \tag{16b}$$

The primes in the above equations denote differentiation with respect to η. It is noted that the unknown core temperature T_o is included in Equation 15. Generally the effect of the values $\partial f/\partial x$ and $\partial\theta/\partial x$ in Equation 14 is dependent on the selection of the similarity variables. Nevertheless, it is still assumed that the values $\partial f/\partial x$ and $\partial\theta/\partial x$ are negligibly small compared with other terms in Equation 14. The possible discrepancy, owing to inexact selection of the similarity variable in the core structure, will be discussed in a later portion of this section. With these approximations, all derivatives with respect to x vanish, and Equation 14 reduces to the one having the so-called *local similarity solution* characteristic:

$$\theta'' + \frac{f\theta'}{2}\left[1 + \frac{I(x)}{n}\right] - f'\theta I(x) = -f'I(x) \tag{17}$$

As is well known, a constant temperature at infinity (T_o = constant) yields a similarity solution with $\psi(x,\eta) = x^{1/2}\psi(\eta)$. The similarity solution for a natural flow along a vertical plate has been studied by Chen and Chen (1988). However, for a porous cavity, the temperature distribution at the core region $T_o(x)$ is unknown and certainly not constant. The steps to determine the core structure $T_o(x)$ by using the integral method are outlined below.

Integrating the momentum equation (Equation 9) with respect to y and making use of the boundary condition (Equation 11), one obtains

$$u = (T - T_o)^{1/n} \tag{18}$$

Integration of Equation 10 with respect to y in combination with Equation 11 yields

$$\frac{d}{dx}\int_0^\infty (T - T_o)^{n+1/n}\,dy + \psi_o\frac{\partial T_o}{\partial x} = -\left.\frac{\partial T}{\partial y}\right|_{y=0} \tag{19}$$

Similarly, integration of the expression $u = \partial\psi/\partial y$ leads to

$$\psi_o = \int_0^\infty (T - T_o)^{1/n}\,dy \tag{20}$$

Equation 20 is substituted into Equation 19 to yield

$$a\frac{d}{dx}(T_o\psi_o) - \psi_o\frac{dT_o}{dx} = -b\frac{T_o^{n+1/n}}{\psi_o} \tag{21}$$

where

$$a = \frac{\int_0^\infty \theta^{n+1/n}(x,\eta)d\eta}{\int_0^\infty \theta^{1/n}(x,\eta)d\eta}, \quad b = -\theta'(x,0)\int_0^\infty \theta^{1/n}(x,\eta)d\eta \tag{22}$$

Obviously, a and b are functions of power-law index n and x respectively. They can be determined if the local similarity temperature profile $\theta(x,\eta)$ is given. It is noted that from the preceding calculations, $a(x)$ and $b(x)$ are found to be weak functions of x. To simplify the procedure, the values of a and b are taken at $x = 1/2$, and then they are considered as constants in the following analysis.

Equation 21 provides a single relationship between the unknowns ψ_o and T_o that governs the core structure of the cavity. A second relationship can be obtained from the boundary-layer solution for the hot wall. Using the centrosymmetry characteristic of the problem, T_o must be odd and ψ_o must be even about the cavity center $x = 1/2$, or

$$T_o(x) = 1 - T_o(1 - x), \quad \psi_o(x) = \psi_o(1 - x) \tag{23}$$

The second integral form of the energy equation for the hot wall shows that

$$a\frac{d}{dx}[(1 - T_o)\psi_o] + \psi_o\frac{dT_o}{dx} = b\frac{(1 - T_o)^{n+1/n}}{\psi_o} \tag{24}$$

From Equations 21 and 24, one can further obtain

$$\frac{a-1}{a}\psi_o\frac{dT_o}{d\psi_o} = \frac{T_o^{n+1/n}(1 - T_o) + T_o(1 - T_o)^{n+1/n}}{T_o^{n+1/n} - (1 - T_o)^{n+1/n}} \tag{25}$$

such that

$$\psi_o = c\frac{[T_o(1 - T_o)]^{(1-a)/a}}{[T_o^{1/n} + (1 - T_o)^{1/n}]^{n(1-a)/a}} \tag{26}$$

where c is the integration constant.

Consequently, from Equation 26, if $\psi_o = 0$ on the horizontal boundaries, it is necessary that

$$T_o(0) = 0, \quad T_o(1) = 1 \tag{27}$$

The following ordinary differential equation can be obtained from Equations 25 and 26:

$$\frac{dT_o}{dx} = \frac{b}{(1-a)c^2}\frac{[T_o^{1/n} + (1 - T_o)^{1/n}]^{1+2n(1-a)/a}}{[T_o(1 - T_o)]^{(2-3a)/a}} \tag{28}$$

The coefficients in the above equation can be determined by integrating it and using the condition of Equations 27:

$$d = \frac{b}{(1-a)c^2} = \sum_0^1 \frac{[\xi(1 - \xi)]^{(2-3a)/a}}{[\xi^{1/n} + (1 - \xi)^{1/n}]^{1+2n(1-a)/a}}\,d\xi \tag{29}$$

The coefficients of a, b, c, and d are functions of the power-law index n.

By setting the value of T_o (it can simply be chosen as $T_o = 1$ at the first step), Equation 13 and 17 together with the boundary condition (Equation 16) were solved using the second-order Runge–Kutta method in order to obtain the dimensionless $f(\eta)$ and $\theta(\eta)$. The new value of T_o was then evaluated by solving Equation 28, in which a and b were determined from Equation 22 with Simpson's integration scheme. The procedure was repeated until a convergent solution was reached.

It must be mentioned that, for the special case of a Newtonian fluid ($n = 1$), Simpkins and Blythe (1980) developed an integral relation approach to study natural convection in porous cavities. The core temperature profile was seen as a function of η only, i.e., $[\theta(\eta)]$. Unfortunately, the profile $\theta(\eta)$ needs to be specified in advance, and then a and b are determined from the specified temperature profile by Equation 22. Therefore, the way of specifying $\theta(\eta)$ is of importance. For the case of $n \neq 1$, it is more difficult to properly propose this kind of a core structure.

The stream function at the center of the core region, or the maximum stream function in the cavity, can be derived by setting $T_o = 1/2$ in Equation 26:

$$\psi_o(\tfrac{1}{2}) = \psi_{max} = c(\tfrac{1}{2})^{(1+n)(1-a)/a} \tag{30}$$

Table 1 *Maximum stream function for various power-law indexes n*

n	0.6	0.8	1.0	1.2	1.4
Ψ_{max}	0.530	0.636	0.730	0.801	0.868

The values for different power-law indexes are given in Table 1.

Figures 2 and 3 show the distributions of the core structure for different power-law indexes n as predicted by the present boundary-layer analysis. The points in these graphs are the results obtained by Simpkins and Blythe (1980) while studying the case of Newtonian fluids ($n = 1$). Very good agreement is observed between the present study and their solution for both the core-temperature and stream-function profiles. It is seen from Figure 2 that the core-temperature distributions are almost unaffected by the value of the power-law index. The solutions exhibit centrosymmetrical properties as expected, and the value of T_o is 0.5 at $x = 1/2$, where the three curves intersect. The curves are seen to be close to a straight line in the central part of the layer. The smaller the power-law index n is, the smaller is the temperature gradient in that region. It is also noted that the temperature gradients are not equal to zero at the horizontal boundaries. As a matter of fact, the core solution is not affected by the thermal characteristics of the horizontal surfaces. For the case of Newtonian fluids, a detailed discussion on the effects of the horizontal boundary conditions is available from Bejan (1979).

Figure 3 shows the variation of the core stream function for the case of non-Newtonian fluids. Its value at the two horizontal boundaries is set equal to 0 by Equation 27. A larger power-law index n yields a smaller value of the core stream function. Its maximum value, ψ_{max}, occurs at the center of cavities. The detailed data of ψ_{max} with different power-law indexes have been listed in Table 1.

In terms of the variables already defined, the Nusselt number representing the amount of heat transfer across the enclosure (Equation 7) can be written as

$$\mathrm{Nu} = \frac{R^{1/2n}}{A^{1/2}} \int_0^1 \left.\frac{\partial T}{\partial y}\right|_{y=0} dx \tag{31}$$

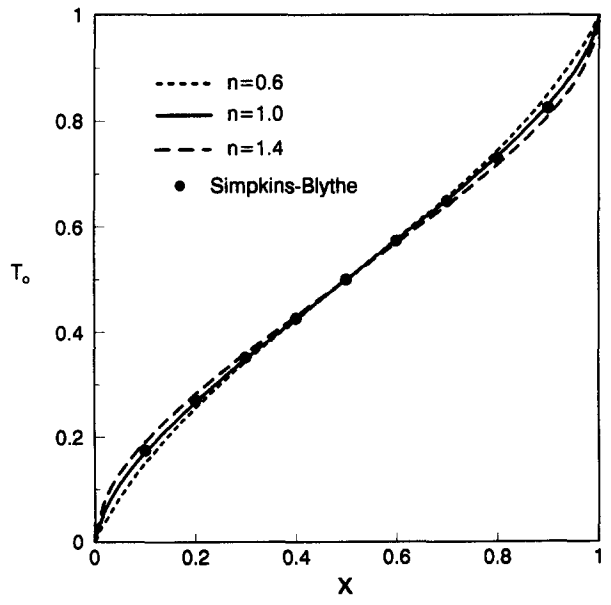

Figure 2 The core temperature profile

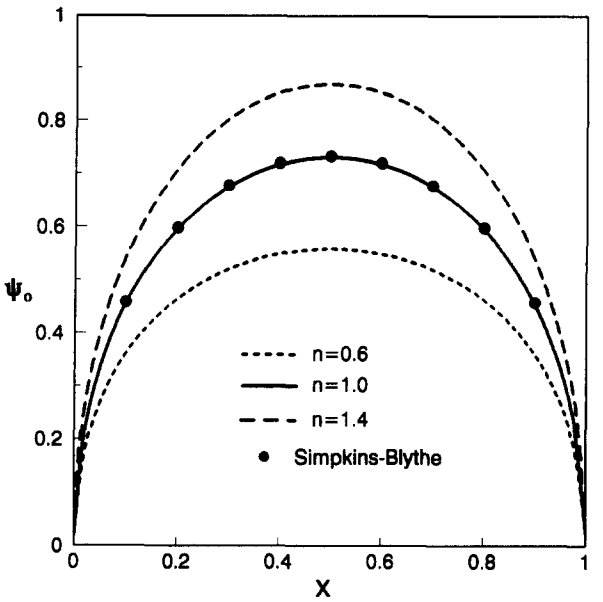

Figure 3 The core stream function

Based on the definition of similarity variables, the Nusselt number can be further expressed as

$$\mathrm{Nu} = \frac{B^*}{A^{1/2}} R^{1/2n} \tag{32}$$

where

$$B^*(n) = \int_0^1 b \frac{T_o^{n+1/n}}{\psi_o} dx \tag{33}$$

is a function of the power-law index n only.

Substituting Equation 26 into Equation 33 and using Equation 28, one obtains

$$B^*(n) = (1-a)c \int_0^1 \frac{\xi^{(n+a)/an}(1-\xi)^{(1-a)/a-1}}{[\xi^{1/n} + (1-\xi)^{1/n}]^{1+(n(1-a)/a)}} d\xi \tag{34}$$

For the case of Newtonian fluids, $n = 1$, the above equation reduces to

$$B^* = (1-a)c \int_0^1 \xi^{1/a}(1-\xi)^{(1/a)-2} d\xi$$

$$= (1-a)cB\left(\frac{1}{a}+1, \frac{1}{a}-1\right) \tag{35}$$

where B is the beta function.

Equation 35 is the same as that developed by Simpkins and Blythe (1980) while studying the flow of Newtonian fluids in a porous cavity with an integral method. However, in the present study, a and b are determined from the coupled Equations 17 and 28.

B^*, as a function of the power-law index n only, is listed in Table 2. For $n = 1$, the result of $B^*(0.509)$ is very vlose to the value 0.51 reported by Simpkins and Blythe (1980) and the value 0.51 ± 0.01 of Walker and Homsy (1978). For convenience, based on the results in Table 2, B^* is further

Table 2 Variation of the coefficient B^* with the power-law index n

n	0.6	0.8	1.0	1.2	1.4
B^*	0.394	0.457	0.509	0.552	0.588

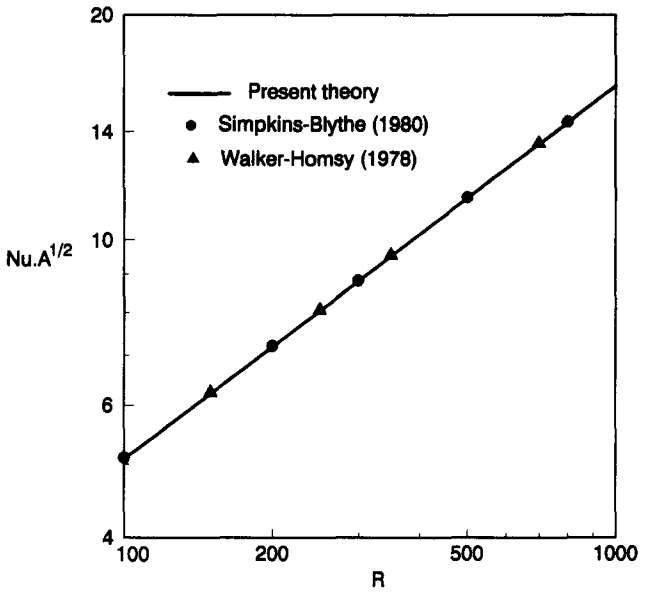

Figure 4 Nusselt number as a function of R for a Newtonian fluid ($n = 1$)

correlated into a function of n in a polynomial form as follows:

$$B^*(n) = 0.153 + 0.475n - 0.117n^2 \tag{36}$$

which is suitable for the boundary-layer regime in the range of $n = 0.6$ to 1.4.

Figure 4 shows a detailed comparison of the averaged Nusselt number, Nu, between the present method and the previous theories for the case of a Newtonian fluid. The results of Simpkins and Blythe (1980) are based on an integral method for the boundary-layer structure, while those of Walker and Homsy (1978) are based on the self-consistent boundary-layer theory obtained by transforming the boundary equations into Blasius coordinates and solving with a numerical technique. The Nusselt number results for both theories have a form similar to that Equation 32, i.e., the Nusselt number Nu is proportional to $(R/A)^{1/2}$. An excellent agreement between the present study and these two theories is observed.

Finally, it must be mentioned that the same similarity variables are used as those introduced by Nakayama and Koyama (1991) in their study of natural convection along a nonisothermal body. However, it is noted that the core structure and heat transfer rate are influenced by the solution of similarity temperature profile θ only through the parameters a and b. Since the parameters a and b are defined in terms of the integral across the layer (see Equation 22), the dependence of the overall core structure on the precise form of $\theta(x, \eta)$ is relatively weak. Thus the selection of the similarity variables for the present problem is not too important, since an integral procedure is used. This conclusion has been demonstrated in the past by the analysis of Simpkins and Blythe (1980) while studying the case of Newtonian fluids. They showed that the selection of three different profiles resulted in a negligible effect on the core structure and heat transfer through the cavity.

Numerical solution

In this section we present a numerical solution of the complete governing equations (Equations 1 to 5). This solution, which can handle both boundary-layer flows (high R) and flows without distinct boundary layers (low R), will be used to determine the accuracy of the approximate analytical boundary-layer solution.

The governing equations (Equations 1 to 5) were solved using the control volume finite-difference method described by Patankar (1980). The variables T^*, ψ^*, u^*, and v^* are used in a staggered grid system. The computational domain is divided into rectangular control volumes with one grid point located at the center of the control volume that forms a basic cell. Temperature T^* and stream function ψ^* are calculated at these grid points. Velocities u^*, v^*, and the dimensionless viscosity coefficient μ_a^* are calculated for points that lie on the faces of these basic cells.

Nonuniform grids are used in the program, allowing a fine grid spacing near the two vertical walls, especially for the case of large Rayleigh numbers R and lower power-law index n. Trial calculations were necessary to optimize the computation time and accuracy. Convergence with mesh size was verified by employing coarser and finer grids on selected test problems. In this study, the values of n are varied from 0.6 to 1.4, which include shear-thinning ($n < 1$) and shear-thickening ($n > 1$) fluids. The approximate boundary-layer solution, developed in the previous section, is valid asymptotically in the limit of a shallow cavity and for high Rayleigh numbers. Therefore, the Rayleigh number is varied from 10^2 to 10^3, and the two aspect ratios $A = 4$, 8 are chosen for the numerical calculations. The computations reported in this paper have been performed on a 61×41 grid for $A = 4$, which has found to model accurately the flow fields described in the results for most of the cases considered. For instance, when $R = 1{,}000$, $A = 4$, and $n = 1.0$, Nusselt numbers of 8.05 and 8.02 and maximum stream functions of 45.05 and 45.07 were obtained with 61×41 and 81×61 meshes, respectively. For $A = 8$, a mesh of 61×61 was utilized.

The criterion used for the iterative convergence is

$$\max \frac{|f_{i,j\text{new}} - f_{i,j\text{old}}|}{|f_{i,j\text{old}}|} < r_f \tag{37}$$

where r_f has been taken as 10^{-4} for ψ^* and 10^{-6} for T^*. The solutions are obtained at a sequence of Rayleigh numbers for a given n.

Figures 5 and 6 show typical streamline and temperature fields obtained numerically for non-Newtonian fluids with the power-law index of $n = 0.6$, 1, and 1.4, respectively. The values of the Rayleigh number, $R = 10^2$ and 10^3, have been selected to represent the asymptotic flow and the boundary-layer regimes, respectively. The streamlines (left) are equally spaced with specified increments $\Delta\psi^*$ between a value of zero on the

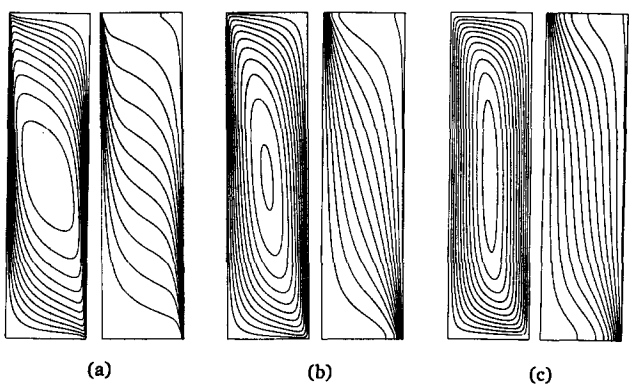

Figure 5 Numerical solutions for the flow and temperature fields $A = 4$, $R = 100$. (a) $n = 0.6$, $\psi^* = 44.1$; (b) $n = 1.0$, $\psi^* = 10.6$; (c) $n = 1.4$, $\psi^* = 2.9$

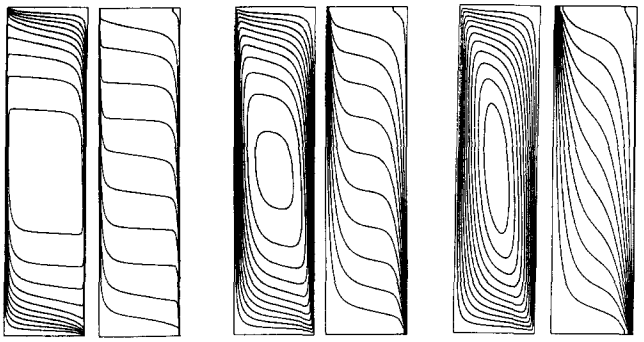

Figure 6 Numerical solutions for the flow and temperature fields $A = 4$, $R = 1000$. (a) $n = 0.6$, $\psi^* = 317.2$; (b) $n = 1.0$, $\psi^* = 45.0$; (c) $n = 1.4$, $\psi^* = 13.8$

boundaries and the extreme value ψ^*_{max} at the center. The isotherms (right) are also equally spaced between zero (left vertical wall) and one (right vertical wall). The dimensionless temperature at the center of the cavity is equal to one half, due to the centrosymmetric character of the problem. The streamlines are observed to be closely spaced near the solid boundaries in both cases $R = 10^2$ and $R = 10^3$. This configuration indicates that, as expected, the fluid velocity is a maximum on the boundaries, since Darcy's law allows the fluid to slip on them. It is also observed that the streamlines become relatively more sparsely spaced near the solid boundaries and the isotherms in the core region are more flat at the higher values of the Rayleigh number R. Isotherms and streamlines are spaced closer together near the right bottom corner and the left top corner, which correspond to the maximum velocity and local heat transfer rate respectively.

A significant change in the velocity and temperature fields is found with a change in power-law index n at a given Rayleigh number R. The shear-thinning fluid ($n = 0.6$) tends to increase the flow circulation within the cavity, making the boundary layer thinner near the two vertical walls and the core fluid more stagnant as compared with the Newtonian fluid ($n = 1$). On the other hand, the shear-thickening fluid ($n = 1.4$) tends to slow down the flow. For instance, it can be seen from Figure 5c that for $R = 100$, the isotherms are almost parallel to the vertical walls, indicating that the circulation within the cavity is weak and heat transfer is almost by pure conduction (asymptotic regime). The maximum stream function, ψ^*_{max}, which is a direct measure of the magnitude of the circulation, decreases from 44.1 to 2.9 as n is increased from 0.6 to 1.4 when $R = 100$. Also, it is seen from Figures 5 and 6 that the smaller the power-law index n, the smaller is the Rayleigh number required for the boundary-layer regime to start. On the other hand, for $n = 1.4$, a relatively large Rayleigh number is required for the boundary-layer regime to start. Thus, it is seen from Figure 6c that, even for a Rayleigh number as high as $R = 10^3$, a relatively weak boundary-layer structure is reached. The slope of the axis of the cells changes with n. For example, at $R = 10^2$, the axis of flow field is below the diagonal of the cavity for $n = 0.6$, but with an increase in n the axis moves towards the vertical middle plane. Therefore, when the Rayleigh number is larger or the power-law index is smaller, the boundary-layer thickness on the vertical walls is thinner and the convection in the cavity is stronger. It should be noted that the flows in the cavity are always unicellular in the range of parameters considered.

Of engineering interest is the total heat transfer rate across the cavity, which is presented in terms of the Nusselt number, defined as

$$\mathrm{Nu} = \frac{1}{A}\int_0^A \left.\frac{\partial T^*}{\partial y^*}\right|_{y^*=0} dx^* \tag{38}$$

Note that the actual heat transfer rate is referenced to the heat transfer by conduction. The above equation was used to evaluate Nu numerically.

Figure 7 shows the effect of the Rayleigh number, R, on the averaged Nusselt number Nu for different power-law indexes n. The coordinate system was set according to the prediction of the scaling analysis. The boundary-layer solution, represented by Equation 32, is illustrated with solid lines. They are straight lines in the selected coordinates and the slopes are different, depending on the power-law index. The points represent the results of the numerical solution. The two aspect ratios $A = 4$ and 8 have been chosen to check the accuracy of the present analytical solution. Generally, a very good agreement between the boundary-layer solution and the numerical simulations is observed from Figure 7 for both cases $A = 4$ and 8. Nevertheless, small differences are seen at low Rayleigh numbers and large power-law indexes. These can be explained as the failure of the boundary-layer assumption. As discussed earlier, a larger power-law index requires a larger Rayleigh number for the boundary-layer regime to start.

Conclusions

Steady natural convection in a rectangular cavity saturated with non-Newtonian fluids is considered based on the modified Darcy power-law model of Pascal (1983). In the boundary-layer regime, a new consistent theory is proposed that is valid for non-Newtonian fluids. The average Nusselt number has been obtained as a function of the Rayleigh number and power-law index of fluids. The results obtained for the special case of a Newtonian fluid are found to be in good agreement with those available in the literature. A numerical study of the same phenomenon, obtained by solving the complete system of governing equations, is also conducted. Two aspect ratios, $A = 4$ and $A = 8$, are chosen to check the results of the proposed analytical method. A good agreement between the

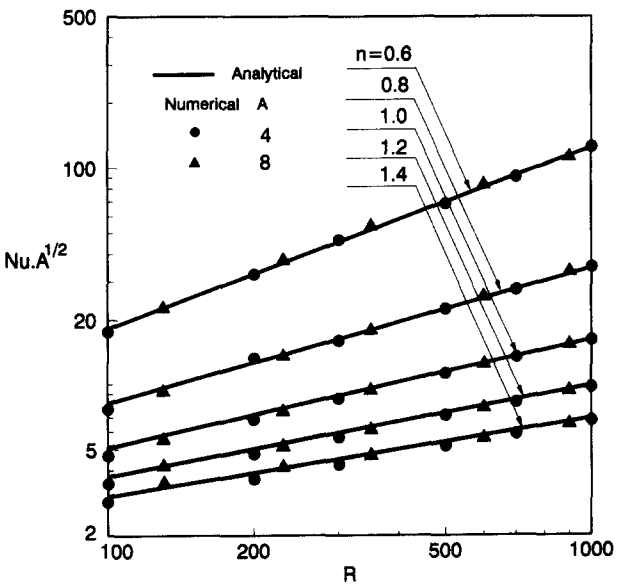

Figure 7 Variation of the overall Nusselt number for different power-law indexes

boundary-layer solution and numerical simulations are found in the range of Rayleigh numbers considered. The power-law index n is observed to influence the temperature and flow fields significantly. For a given R, the boundary-layer flow regime reverts to the asymptotic and then to the conduction regime as the power-law index n is increased, while the heat transfer rate through the vertical walls greatly increases as the power-law index is decreased.

References

Amari, B., Vasseur, P., and Bilgen, E. 1994. Natural convection of non-Newtonian fluids in a horizontal porous layer. *Warme-und stoffubertragung*, **29**, 185–193

Bejan, A. 1979. On the boundary layer regime in a vertical enclosure filled with porous medium. *Lett. Heat Mass Transfer*, **6**, 93–102

Bejan, A. 1985. The method of scale analysis in porous media. *Natural Convection: Fundamentals and Application*. Hemisphere, Washington, DC, 548–572

Bian, W., Vasseur, P., and Bilgen, E. In press. Natural convection of non-Newtonian fluids in an inclined porous layer. *Chem. Eng. Comm.*

Chen, H. T. and Chen, C. K. 1987. Natural convection of non-Newtonian fluids about a horizontal surface in a porous medium. *J. Energy Res. Technol.*, **109**, 119–123

Chen, H. T. and Chen, C. K. 1988a. Natural convection of non-Newtonian fluids in the porous medium on a horizontal surface. *Chem. Eng. Comm.*, **69**, 29–41

Chen, H. T. and Chen, C. K. 1988b. Free convection of non-Newtonian fluids along a vertical plate embedded in a porous medium. *J. Heat Transfer*, **110**, 257–260

Christopher, R. V. and Middleman, S. 1965. Power-law flow through a packed tube. *Ind. Eng. Chem. Fund.*, **4**, 422–426

Dharmadhikari, R. V. and Kale, D. D. 1985. Flow of non-Newtonian fluids through porous media. *Chem. Eng. Sci.*, **40**, 527–529

Gill, A. E. 1966. The boundary layer regime for convection in a rectangular cavity, *J. Fluid Mech.*, **26**, 515–536

Nakayama, A. 1992. Non-Darcy couette flow in a porous medium filled with an inelastic non-Newtonian fluid. *J. Fluids Eng.*, **114**, 642–647

Nakayama, A. and Koyama, H. 1991. Buoyancy-induced flows of non-Newtonian fluids over a non-isothermal body of arbitrary shape in a fluid-saturated porous medium. *Appl. Sci. Res.*, **48**, 55–70

Nield, D. A. and Bejan, A. 1992. *Convection in Porous Media*. Springer Verlag, New York

Pascal, H. 1983. Rheological behavior effect of non-Newtonian fluids on steady and unsteady flow through porous media. *Int. J. Numer. Anal. Methods Geomech.*, **7**, 207–224

Pascal, H. and Pascal, J. P. 1989. Nonlinear effects of non-Newtonian fluids on natural convection in a porous medium. *Physica D*, **40**, 393–402

Patankar, S. 1980. *Numerical Heat Transfer and Fluid Flow*. Hemisphere, New York

Simpkins, P. G. and Blythe, P. A. 1980. Convection in a porous layer. *Int. J. Heat Mass Transfer*, **23**, 881–887

Walker, K. L. and Homsy, G. M. 1978. Convection in a porous cavity. *J. Fluid Mech.*, **87**, 449–474

Weber, J. E. 1975. The boundary-layer regime for convection in a vertical porous layer. *Int. J. Heat Mass Transfer*, **18**, 569–573